PHYSICAL REVIEW E VOLUME 53, NUMBER 1 JANUARY 1996

Kolmogorov's refined similarity hypothesis for hyperviscous turbulence

Vadim Borue and Steven A. Orszag
Fluid Dynamics Research Center, Princeton University, Princeton, New Jersey 08544-0710
(Received 13 September 1995)

Kolmogorov's refined similarity hypothesis (RSH) is tested in high resolution numerical simulations of forced three-dimensional homogeneous turbulence. High Reynolds numbers are achieved by using hyperviscous dissipation $(-1)^{h+1}\Delta^h$ $(h=8)$ instead of Newtonian $(h=1)$ dissipation. It is found that, in the inertial range, the RSH is reasonably well satisfied for low order moments with noticeable systematic corrections for higher order moments. Within the constraints imposed by the use of hyperviscosity our data nearly eliminate trivial kinematic dependencies between longitudinal velocity differences and the energy dissipation rate thus helping to reveal the true dynamical nature of the RSH.

PACS number(s): 47.27.Ak, 47.27.Gs, 47.27.Jv

One of the most interesting properties of fully developed turbulence is small scale intermittency which manifests itself through the scale dependence of the probability distribution function (PDF) $\mathscr{P}(\Delta u_r/r^{1/3})$ of longitudinal velocity differences $(\Delta u_r=[u_i(x+r)-u_i(x)]r_i/r)$. In order to take account of this intermittent behavior, Kolmogorov [1] introduced the refined similarity hypothesis (RSH) which relates velocity differences Δu_r and the locally averaged energy dissipation rate

$$\mathscr{E}_r(x)=\int F_r(\mathbf{x}-\mathbf{y})\mathscr{E}(\mathbf{y})d^3y, \tag{1}$$

where $\mathscr{E}(\mathbf{y})$ is the local energy dissipation rate and F_r is a low-pass spatial filter with scale r and normalized, $\int F_r(x)d^3x=1$. The RSH states that the joint one-point PDF of Δu_r and $\mathscr{E}_r$ has the form

$$\mathscr{P}(\Delta u_r,\mathscr{E}_r)=\mathscr{P}_v\left(V_r\equiv\frac{\Delta u_r}{r^{1/3}\mathscr{E}_r^{1/3}}\right)\mathscr{P}_{\mathscr{E}}(\mathscr{E}_r) \tag{2}$$

and that, in the inertial range, the PDF $\mathscr{P}_v(V_r)$ is independent of scale and Reynolds number. The RSH is the basis of nearly all existing cascade models of turbulence (see, e.g., [2]).

Recently, the RSH was independently checked experimentally by four groups [3–6] all concluding that, on the level of the first conditional moment, the RSH has solid experimental support, i.e., the conditional average of $\langle|V_r||\mathscr{E}_r\rangle$ is relatively independent of $\mathscr{E}_r$. In all these works, a one-dimensional surrogate of real dissipation was used and local averaging of $\mathscr{E}$ was understood as one-dimensional averages. It was suggested in [7] that at least part of the observed correlations between Δu_r and $\mathscr{E}_r$ come from the measurement procedures that emphasize the kinematic dependence between these two quantities. Thoroddsen [8] attempts to verify the RSH by eliminating kinematic dependencies by using pseudodissipation defined via the transverse velocity component. It was suggested in [8] that with this definition of the dissipation rate the validity of the RSH is questionable. Existing numerical simulations [9,10] give only partial support of the RSH, but unfortunately employed many of the same simplifications to calculate $\mathscr{E}_r$ as used in experiments [with either the one-dimensional pseudodissipation $15\nu(\partial u/\partial x)^2$ or anisotropic one-dimensional local averaging being used]. Recent numerical simulations [11] aimed to eliminate kinematic factors but give only weak support of the RSH.

In this work, we present evidence supporting the RSH at least at the level of low order moments that is free from the kinematic constraints discussed above. In previous works [12–14] we have already demonstrated that for the same numerical resolution, we can effectively increase the extent of the inertial range of three-dimensional turbulence by an order of magnitude by using alternative forms of dissipation. Some evidence was given that three-dimensional inertial-range dynamics is relatively independent of the form of the hyperviscosity, although it may depend on the nature of the force. In this Rapid Communication, we address the problem of validation of the RSH.

The hyperviscosity-modified Navier-Stokes equations are

$$\partial_t u_i+u_j\partial_j u_i=-\partial_i p+(-1)^{h+1}\nu_h\Delta^h u_i+f_i, \tag{3}$$

where the pressure p is calculated from the incompressibility condition $\partial_i u_i=0$. We include a white-in-time Gaussian force which is nonzero only at some characteristic scale $k_f=1$ and a hyperviscosity dissipation (as in [12] we use $h=8$). The various characteristics of the statistically stationary state in this case can be found in [12]. We solve (3) using a pseudospectral parallel code and perform two series of runs with resolutions $(N=128)^3$ and 256^3 for a periodic box with size $L=2\pi$ in each direction. The total averaging times are 200 and 30 in units $\tau_0\approx 1/v_{rms}$, respectively. The Reynolds number [12] is $R_\lambda\approx 50(k_d/k_f)^{2/3}$, where k_d is the wave number where $k^2E(k)$ is maximum ($k_d\approx 41{,}82$ for 128^3 and 256^3). The hyperviscous energy dissipation rate is

$$\mathscr{E}=\nu_h\Delta^{h/2}u_i\Delta^{h/2}u_i. \tag{4}$$

The local space average in (1) is performed as a convolution in Fourier space by using an isotropic three-dimensional "top-hat" low-pass filter whose Fourier transform is $F_r(\mathbf{k})=3(\sin\xi-\xi\cos\xi)/\xi^3$ with $\xi=r|\mathbf{k}|/2$. This filter exactly corresponds to the definition of local space averaging used by Kolmogorov [1]. The midpoint of the velocity difference

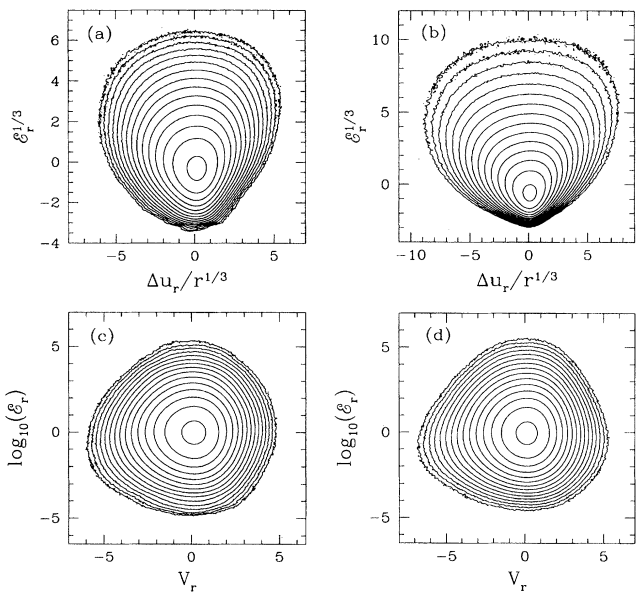

FIG. 1. Joint PDFs between [(a),(b)] $\Delta u_r/r^{1/3}$ and $\mathscr{E}_r^{1/3}$; [(c),(d)] V_r and $\log_{10}\mathscr{E}_r$. Means are subtracted and variables are normalized by their variances. [(a),(c)] $k_c=4$ and resolution 128^3. [(b),(d)] $k_c=32$ and resolution 256^3. The total number of points is $\approx 10^{10}$. Curves show isocontours of $\log_{10}\mathscr{P}$ in increments of 0.4.

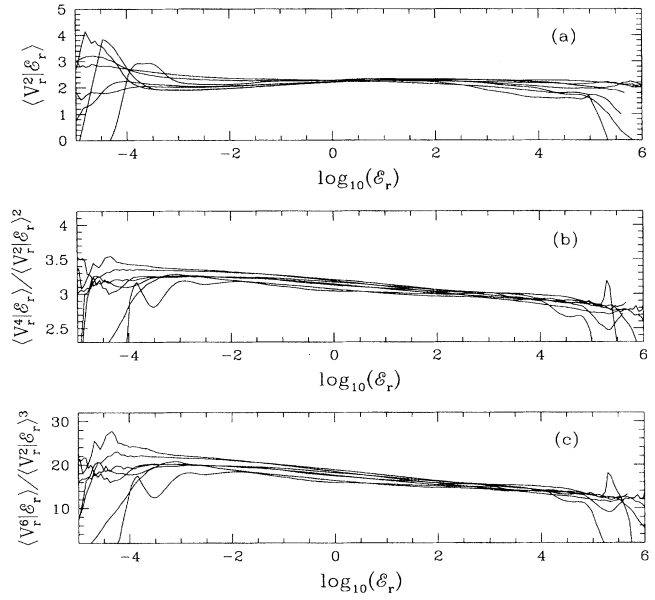

FIG. 2. (a) Conditional averages of $\langle V_r^2|\mathscr{E}_r\rangle$; (b) conditional flatness $\langle V_r^4|\mathscr{E}_r\rangle/\langle V_r^2|\mathscr{E}_r\rangle^2$; (c) conditional sixth order moments $\langle V_r^6|\mathscr{E}_r\rangle/\langle V_r^2|\mathscr{E}_r\rangle^3$. Curves are obtained for 128^3 and 256^3 resolutions with $k_c=4,8,16$ and $k_c=4,8,16,32$, respectively. All curves are superimposed with the dissipation rate plotted as $(\log_{10}\mathscr{E}_r-\langle\log_{10}\mathscr{E}_r\rangle)/\sigma_r$ (σ_r^2 is the variance of $\log_{10}\mathscr{E}_r$).

Δu_r coincides with the center of the spherical averaging cell of radius $r/2$. The definition of dissipation (4) and this measurement procedure nearly eliminate the possible kinematic dependencies discussed above. The measurements are carried out for $r=\pi/k_c$ with $k_c=4,8,\ldots,N/8$ which correspond to scales inside of the inertial range [12].

In Fig. 1 we plot the joint probability distribution functions $\mathscr{P}_u(\Delta u_r/r^{1/3},\mathscr{E}_r^{1/3})$ [Figs. 1(a) and 1(b)] and $\mathscr{P}(V_r,\log_{10}\mathscr{E}_r)$ [Figs. 1(c) 1(d)] for two spatial resolutions and filter sizes: $k_d=41,82$ and $k_c=4,32$. While isocontours of $\mathscr{P}_u$ indicate a noticeable correlation of velocity differences and the dissipation rate, isocontours of $\mathscr{P}$ show that V_r and $\log_{10}\mathscr{E}_r$ are nearly statistically independent in accordance with the RSH. To quantify this we calculate conditional moments of V_r conditioned on $\mathscr{E}_r$. Various moments are plotted in Figs. 2 and 3 as functions of $(\log_{10}\mathscr{E}_r-\langle\log_{10}\mathscr{E}_r\rangle)/\sigma_r$ (σ_r^2 is the variance of $\log_{10}\mathscr{E}_r$). The curves for different r and k_d nearly collapse using the above scaling. These figures show that the conditional moments of V_r are only weakly dependent on $\log_{10}\mathscr{E}_r$ and the RSH in the form (2) is approximately satisfied. The conditional mean $\langle V_r|\mathscr{E}_r\rangle$ is nearly equal to zero in contrast with the results of [6]. The conditional variance $\langle V_r^2|\mathscr{E}_r\rangle\approx 2.2$ is close to the results of [3] and [10]. The conditional flatness [Fig. 2(b)] and conditional sixth order moments [Fig. 2(c)] are only weakly dependent on $\log_{10}\mathscr{E}_r$ and are close to Gaussian values (3 and 15, respectively) in agreement with [3,6,10]. The first and third conditional moments of $|V_r|$ normalized by conditional variances [Figs. 3(a) and 3(b)] are spectacularly independent of $\log_{10}\mathscr{E}_r$ (partially due to the normalization by $\langle V_r^2|\mathscr{E}_r\rangle$). The conditional skewness [Fig. 3(c)] has a substantially stronger dependence on $\log_{10}\mathscr{E}_r$. Also in accordance with Kolmogorov's 4/5 law [3] $\langle V_r^3\rangle$ is nearly equal to $-4/5$.

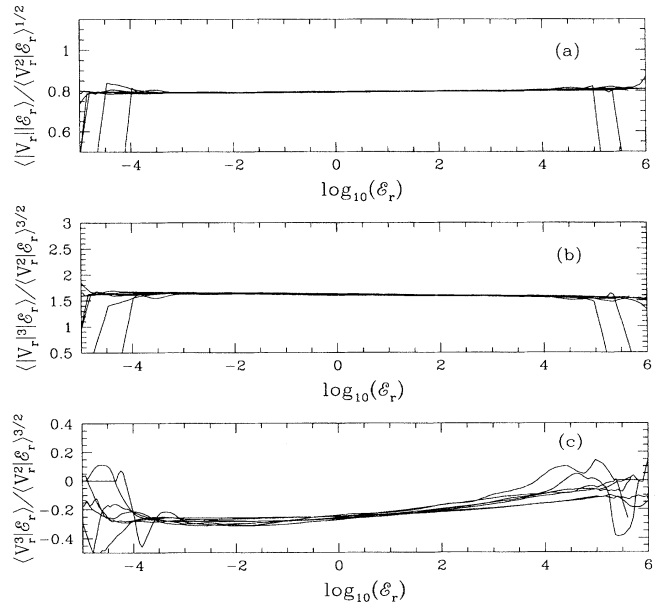

FIG. 3. (a) Conditional averages of $\langle|V_r||\mathscr{E}_r\rangle/\langle V_r^2|\mathscr{E}_r\rangle^{1/2}$; (b) conditional third order moments $\langle|V_r|^3|\mathscr{E}_r\rangle/\langle V_r^2|\mathscr{E}_r\rangle^{3/2}$; (c) conditional skewness $\langle V_r^3|\mathscr{E}_r\rangle/\langle V_r^2|\mathscr{E}_r\rangle^{3/2}$. Curves are obtained for 128^3 and 256^3 resolutions with $k_c=4,8,16$ and $k_c=4,8,16,32$, respectively. All curves are superimposed with the dissipation rate plotted as $(\log_{10}\mathscr{E}_r-\langle\log_{10}\mathscr{E}_r\rangle)/\sigma_r$ (σ_r^2 is the variance of $\log_{10}\mathscr{E}_r$).

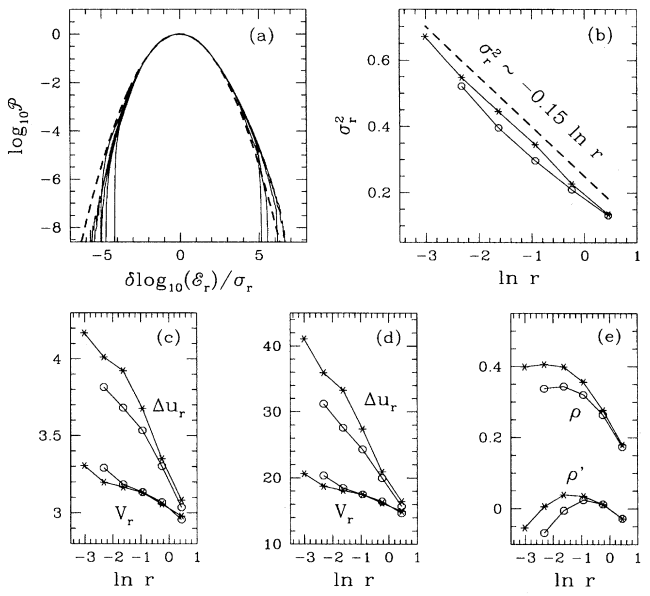

FIG. 4. (a) PDFs of $\log_{10}\mathscr{E}_r$; $\log_{10}\mathscr{P}$ is plotted as a function of $(\log_{10}\mathscr{E}_r-\langle\log_{10}\mathscr{E}_r\rangle)/\sigma_r$. (b) Variance $\tilde{\sigma}_r^2$ of $\ln\mathscr{E}_r$ as a function of filter size $\ln(r)$; the dashed line is $\tilde{\sigma}_r^2\propto-0.15\ln(r)$. (c) Flatness of velocity differences Δu_r and V_r as a function of filter size $\ln(r)$. (d) Sixth order moments $\langle\Delta u_r^6\rangle/\langle\Delta u_r^2\rangle^3$ and $\langle V_r^6\rangle/\langle V_r^2\rangle^3$ as a function of filter size $\ln(r)$. (e) Correlation coefficients ρ between $|\Delta u_r|$ and $\mathscr{E}_r^{1/3}$ and ρ' between $|V_r|$ and $\log_{10}\mathscr{E}_r$ as functions of filter size $\ln(r)$. The measurements are performed for 128^3 and 256^3 resolutions and $k_c=4,8,16$ and $k_c=4,8,16,32$, respectively. All data are superimposed in (a). In (b)–(e) stars represent data for 256^3 resolution and circles represent data for 128^3 resolution.

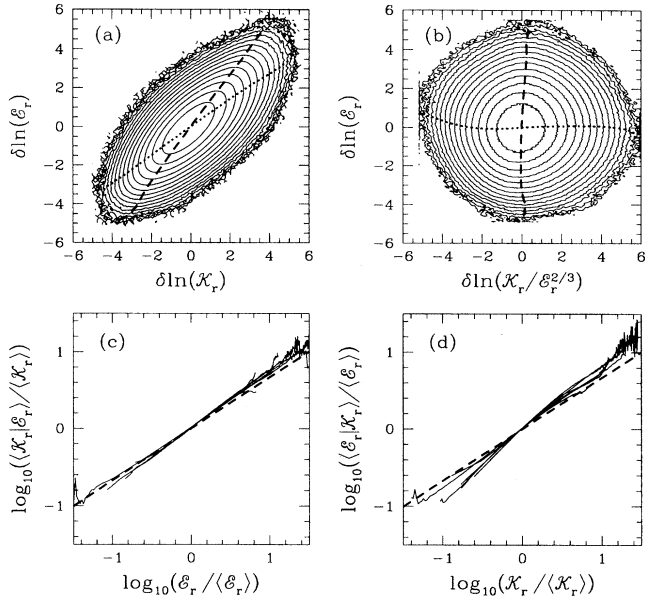

FIG. 5. Joint PDFs between (a) $\ln\mathscr{K}_r$ and $\ln\mathscr{E}_r$, (b) $\ln(\mathscr{K}_r/\mathscr{E}_r^{2/3})$ and $\ln\mathscr{E}_r$. Means are subtracted and variables are normalized by their variances. $k_c=16$ and $k_d=41$. Curves show isocontours of $\log_{10}\mathscr{P}$ in increments of 0.4. Dotted curves are conditional averages of abscissas conditioned on ordinates and dashed curves are vice versa. $\log_{10}$-$\log_{10}$ plots of (c) conditional averages of $\langle\mathscr{K}_r|\mathscr{E}_r\rangle/\langle\mathscr{K}_r\rangle$ as a function of $\mathscr{E}_r/\langle\mathscr{E}_r\rangle$; dashed curve corresponds to $\mathscr{E}_r^{2/3}$ (d) conditional averages of $\langle\mathscr{E}_r|\mathscr{K}_r\rangle/\langle\mathscr{E}_r\rangle$ as a function of $\mathscr{K}_r/\langle\mathscr{K}_r\rangle$; dashed curve corresponds to $\mathscr{K}_r^{2/3}$. Curves are obtained for 128^3 and 256^3 resolutions with $k_c=4,8,16$ and $k_c=4,8,16,32$, respectively. All curves are superimposed.

In Figs. 4(a) and 4(b) we plot the PDFs of $\log_{10}\mathscr{E}_r$ as a function of $(\log_{10}\mathscr{E}_r-\langle\log_{10}\mathscr{E}_r\rangle)/\sigma_r$, superimposed for different r and Reynolds numbers. All curves nearly collapse in the core region with the variance $\tilde{\sigma}_r^2$ of $\ln\mathscr{E}_r$ proportional to $-\mu\ln(r)$ (here $\mu\approx0.15$ is called the intermittency exponent). The PDFs of $\log_{10}\mathscr{E}_r$ are quite close to Gaussian. With our data set it is possible to obtain moments $\langle\mathscr{E}_r^n\rangle$ in the range $-2\leq n\leq4.5$ and within this range the PDF of $\mathscr{E}_r$ may be considered log-normal. If the flatness and sixth moments of Δu_r grow when r decreases the corresponding quantities for V_r grow more slowly and may even slightly decrease when R_λ increases [see Figs. 4(c) and 4(d)]. Note that according to the RSH the correlation coefficient ρ between $|\Delta u_r|$ and $\mathscr{E}_r^{1/3}$ should not be equal to 1. Indeed from (2), $\rho=(1-A)^{1/2}/(B-A)^{1/2}$ with $A=\langle\mathscr{E}_r^{1/3}\rangle^2/\langle\mathscr{E}_r^{2/3}\rangle$ and $B=\langle V_r^2\rangle/\langle|V_r|\rangle^2$. From the data plotted in Figs. 3 and 4, $A\approx1-\tilde{\sigma}_r^2/9$, $B\approx1.56$, and $\rho\approx0.45\tilde{\sigma}_r$. In accord with the RSH, the correlation coefficient ρ' between $|V_r|$ and $\log_{10}\mathscr{E}_r$ is close to zero [see Fig. 4(e)].

If the PDFs of $\log_{10}\mathscr{E}_r$ and V_r are close to Gaussian and the RSH holds, isocontours of $\mathscr{P}_v$ will have the form of circles. That is not exactly so, as may be seen from Fig. 1. Our data not only allow us to validate the RSH on the level of lower order moments, but also reveal systematic corrections to the RSH. Indeed according to the results plotted in Fig. 2(c) $\langle V_r^6|\mathscr{E}_r\rangle\propto a(1-b\ln\mathscr{E}_r/\tilde{\sigma}_r)$ where $a\approx160$ and $b\approx1/15$. That leads to systematic corrections to $\langle\Delta u_r^6\rangle\propto r^2\langle\mathscr{E}_r^\alpha\rangle$ with $\alpha\approx2-b/\tilde{\sigma}_r$ and the RSH is, strictly speaking, violated. The situation is even worse for higher order moments. We do not know whether these systematic corrections to higher order moments are universal and/or hyperviscosity independent.

One may expect that the RSH should not only be applicable to velocity differences, but to other inertial range quantities as well. To illustrate this idea we measure the joint probability distribution of subgrid-scale kinetic energy $\mathscr{K}_r$ and $\mathscr{E}_r$. We define $\mathscr{K}_r$ as $\mathscr{K}_r=\frac{1}{2}[(u_iu_i)_r-(u_i)_r(u_i)_r]$ with the same local-averaging procedure as in (1) and with the same top-hat filter F_r. We have checked that our results are relatively independent on the form of filter. According to the RSH we may expect that

$$\mathscr{P}(\mathscr{K}_r,\mathscr{E}_r)=\mathscr{P}_{\mathscr{K}}\left(\frac{\mathscr{K}_r}{r^{2/3}\mathscr{E}_r^{2/3}}\right)\mathscr{P}_{\mathscr{E}}(\mathscr{E}_r). \tag{5}$$

In Fig. 5(a) we plot $\mathscr{P}(\ln\mathscr{K}_r,\ln\mathscr{E}_r)$ for $k_c=16$ and $k_d=41$. A strong correlation between $\mathscr{K}_r$ and $\mathscr{E}_r$ is observed. It turns out that the probability distribution of $\mathscr{K}_r$ is also approximately log-normal with $\tilde{\sigma}_r^2$, the variance of $\ln\mathscr{K}_r$, nearly equal to $\tilde{\sigma}_r^2$, the variance of $\ln\mathscr{E}_r$ independently of k_c and k_d. Therefore, if the RSH in the form (5) is correct the isocontours of $\mathscr{P}(\ln(\mathscr{K}_r/\mathscr{E}_r^{2/3}),\ln\mathscr{E}_r)$ should have the form of circles. That this is indeed nearly so can be seen from Fig. 5(b).

For further analysis it is convenient to introduce the variables $\xi=(\ln\mathscr{E}_r-\langle\ln\mathscr{E}_r\rangle)/\tilde{\sigma}_r$ and $\eta=(\ln\mathscr{K}_r-\langle\ln\mathscr{K}_r\rangle)/\tilde{\sigma}_r$ with $\tilde{\sigma}_r\approx\tilde{\sigma}_r$. We verified that, in these variables, the joint PDF of $\mathscr{K}_r$ and $\mathscr{E}_r$ in the inertial range has the simple approximate form

$$\mathscr{P}(\mathscr{K}_r,\mathscr{E}_r)\propto\exp\left[-\frac{\xi^2+\eta^2}{2(1-c^2)}+\frac{c\xi\eta}{(1-c^2)}\right] \tag{6}$$

independently of k_c and k_d. Here $\langle\xi^2\rangle=\langle\eta^2\rangle=1$ and $c=\langle\xi\eta\rangle$ is the correlation coefficient. It is clear from (6) that ξ and $\eta-c\xi$ or equivalently $\mathscr{K}_r/\mathscr{E}_r^c$ and $\mathscr{E}_r$ are independent variables. The RSH in the form (5) holds provided $c=2/3$; this turns out to be approximately true according to our data. It follows from (6) that the conditional averages $\langle\eta|\xi\rangle=c\xi$ and $\langle\xi|\eta\rangle=c\eta$. Using the fact that ξ and η are nearly Gaussian variables and that $\tilde{\sigma}_r\approx\tilde{\sigma}_r$ we obtain

$$\langle\mathscr{K}_r|\mathscr{E}_r\rangle\propto\mathscr{E}_r^{2/3},\quad\langle\mathscr{E}_r|\mathscr{K}_r\rangle\propto\mathscr{K}_r^{2/3}. \tag{7}$$

The conditional averages $\langle\mathscr{K}_r|\mathscr{E}_r\rangle$ and $\langle\mathscr{E}_r|\mathscr{K}_r\rangle$ are plotted in Figs. 5(c) and Fig. 5(d), respectively. It may be seen that (7) is approximately satisfied independently of k_c and k_d [with the first expression in Eq. (7) that directly tests the RSH validity with noticeably higher accuracy]. The results (7) are in good agreement with recent experimental findings of Meneveau and O'Neil [15]. Thus, the RSH for $\mathscr{K}_r$ is approximately valid in the form (5); it cannot be inverted in the sense that $\langle\mathscr{E}_r|\mathscr{K}_r\rangle$ does not scale as $\mathscr{K}_r^{3/2}$.

We also checked that the RSH holds for other inertial range quantities such as locally averaged strain and vorticity that are defined as $(S_{ij})_r=[(\partial_i u_j+\partial_j u_i)/2]_r$ and $(\omega_i)_r=\varepsilon_{ijk}\partial_j(u_k)_r$. Here the same filtering procedure is assumed. Precisely, we verified that the joint PDF of $\mathscr{E}_r$ and $S_r^2=(S_{ij})_r(S_{ij})_r$ has the form (5): $\mathscr{P}_S(S_r^2/\mathscr{E}_r^{2/3})\mathscr{P}_{\mathscr{E}}(\mathscr{E}_r)$. The same decomposition is true for the joint PDF of $\mathscr{E}_r$ and locally averaged vorticity $\omega_r^2=(\omega_i)_r(\omega_i)_r$: $\mathscr{P}_\omega(\omega_r^2/\mathscr{E}_r^{2/3})\mathscr{P}_{\mathscr{E}}(\mathscr{E}_r)$. As in the case of subgrid-scale kinetic energy, the RSH for large-scale strain and vorticity cannot be inverted.

In conclusion, we find that in the inertial range, the RSH in the form (2) is reasonably well satisfied for low order moments of velocity differences with noticeable systematic corrections for higher order moments. We have also shown that the RSH is as well applicable to other inertial range quantities such as subgrid-scale kinetic energy, locally averaged strain and vorticity. Our use of hyperviscosity and an accurate averaging procedure allows us to nearly eliminate kinematic dependencies between velocity differences and the dissipation rate, thus helping to reveal the dynamical nature of the RSH. On the other hand, our results also give more confidence to the hypothesis that inertial-range dynamics is relatively independent of the form of hyperviscosity.

We are grateful to V. Yakhot, K. Sreenivasan, and M. Vergassola for valuable discussions. This work was supported by ARPA/ONR under URI Grant No. N00014-92-J-1796, AFOSR Grant No. F49620-93-1-0296, and ONR Contract No. N00014-92-C-0118.

[1] A.N. Kolmogorov, J. Fluid Mech. **13**, 82 (1962).
[2] M. Nelkin, Adv. Phys. **43**, 143 (1994).
[3] G. Stolovitzky, P. Kaliasnath, and K.R. Sreenivasan, Phys. Rev. Lett. **69**, 1178 (1992).
[4] A. Praskovsky, Phys. Fluids A **4**, 2589 (1992).
[5] S.T. Thoroddsen and C.W. Van Atta, Phys. Fluids A **4**, 1592 (1992).
[6] Y. Gagne, M. Marchand, and B. Castaing, J. Phys. (France) II **4**, 1 (1994).
[7] G. Stolovitzky and K.R. Sreenivasan, Rev. Mod. Phys. **66**, 229 (1994).
[8] S.T. Thoroddsen, Phys. Fluids **7**, 691 (1995).
[9] S. Chen, G. Doolen, R. Kraichnan, and Z.-S. She, Phys. Fluids A **5**, 458 (1993).
[10] L.-P. Wang, S. Chen, J. Brasseur, and J. Wyngaard, J. Fluid Mech. (to be published).
[11] S. Chen, G. Doolen, R. Kraichnan, and L.-P. Wang, Phys. Rev. Lett. **74**, 1755 (1995).
[12] V. Borue and S. Orszag, Europhys. Lett. **29**, 687 (1995).
[13] V. Borue and S. Orszag, Phys. Rev. E **51**, R856 (1995).
[14] V. Borue and S. Orszag, J. Fluid. Mech. **306**, 293 (1996).
[15] C. Meneveau and J. O'Neil, Phys. Rev. E **49**, 2866 (1994).